Application of the double optic probe technique to distorted tumbling bubbles in aqueous or organic liquid

H. Chaumat[a], A.M. Billet-Duquenne[a,*], F. Augier[b], C. Mathieu[b], H. Delmas[a]

[a]*Laboratoire de Génie Chimique, Z.A Basso Cambo, 5 rue Paulin Talabot, 31106 Toulouse cedex 1, France*
[b]*Rhodia, Centre de Recherches de Lyon, 85 av. des Frères Perret, B.P 62, 69192 St Fons cedex, France*

Abstract

The optic probe technique is widely used to investigate bubble reactors. To derive values of bubble local velocities and bubble local sizes, a specific signal treatment is usually applied under severe assumptions for bubble path and shape. However, in most industrial reactors, bubble motion is chaotic and no common shape can be assumed.

In this work, the reliability of the signal treatment associated with the optic probe technique is examined for distorted and tumbling bubbles. A double-tip optic probe is settled in a glass tank and the rise of bubbles is filmed simultaneously. Several trains of bubbles are studied, interactions between bubbles being gradually increased.

Referring to image analysis, several ways to derive mean bubble velocities from optic probe data have been compared. Crenels from front tip and rear tip raw signals are associated and individual bubble velocities are derived. Nevertheless, complete velocity distributions are difficult to obtain, as they depend on the choice of the time within which the bubble is searched on the second tip. Using a simpler approach it is shown that the most probable velocity, calculated through the raw signals inter-correlation, is a correct estimation of the average bubble velocity.

Concerning bubble size, bubble chord distributions show too high values due to bubble distortion and deviation. A simplified estimation of bubble mean Sauter diameter, using the most reliable measurements only (i.e., local gas hold-up, local mean bubbling frequency, and most probable bubble velocity), was tested for highly distorted bubbles; this method was validated both in water and cyclohexane.

1. Introduction

The investigation of industrial bubble reactors is classically achieved by measuring the overall gas hold-up and the liquid Residence Time Distribution. Then, global and empirical reactor models are carried out including mass transfer and chemical reaction kinetics. More complex approaches based on computational fluid mechanics codes seem very promising as they could be predictive. Nevertheless, they are still far from reliable as many physical aspects have to be included. The most important information to bring to these codes is the bubble average diameter.

In addition, in bubble flows, small-scale phenomena heavily influence the global performance of the reactor: liquid and bubbles re-circulate in loops, gas-phase distribution is non-uniform, mean bubble size varies because of coalescence or break-up. Distributions of interfacial area, of bubble and liquid velocities, and of chemical species concentrations have to be taken into account for a better understanding of bubble reactors performance.

In the last two decades, experimental efforts have been made towards local investigations inside these multiphase reactors (Boyer et al., 2002). Metal walls and high bubble number density in large pilots do not allow the use of

* Corresponding author. Tel.: +33 534615256; fax: +33 534615253.
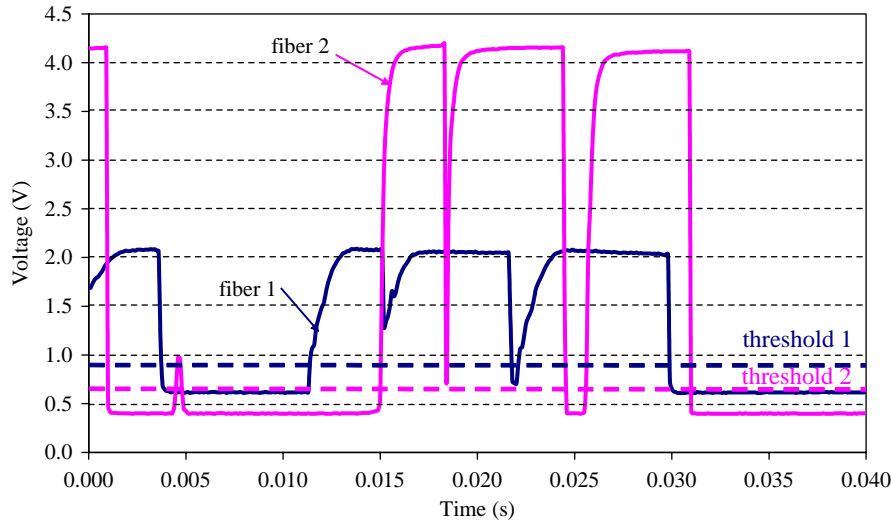*E-mail address:* AnneMarie.Billet@ensiacet.fr
(A.M. Billet-Duquenne).

Fig. 1. Simultaneous raw signals delivered by a double optic probe.

visualisation techniques or Doppler techniques. Though invasive, the optic probe is used as it is quite easy to settle through reactors walls and can be applied even with non-conductive liquids, as industrial organic solvents (Boyer and Cartellier, 1999). The optic probe delivers a near square-pulsed raw signal (Fig. 1); pulses correspond to the residence of bubbles around the optic fibre tip. Therefore, local values of gas hold-up and bubbling frequency can be easily deduced by signal treatment. Using a double-tip optic probe, bubble velocity and bubble size can also be estimated, under statistical considerations and very restrictive assumptions: bubbles are supposed to rise vertically and they are considered as spheres or ellipsoïds (Kamp et al., 1995). Note that, even if the shape of bubbles is controlled and if bubbles rise isolated in quiet liquid, their motion is not strictly vertical and the physical interaction between probe and bubbles leads to measurement discrepancies (Ellingsen and Risso, 2001; Kiambi et al., 2003).

In industrial bubble reactors the above-mentioned restrictive assumptions are far from verified: flows are chaotic, the non-uniformity in gas dispersion generates small- and large-scale liquid loops, bubbles wakes create liquid vortices and increase turbulence intensity and shear stress. As a consequence, bubbles tumble around in these reactors and are highly distorted. Consistence of optic probe signal treatment becomes questionable:

- In what way does the lateral motion of bubbles influence bubble-probe measurement?
- In what way does the continuous deformation of bubble interface modify the residence time of bubble on probe tip, and the flying time between probe tips?

This work is focused on the reliability of optic probe signal treatment in complex flow conditions. As a first stage of validation and to avoid problems due to very high bub-

ble concentration, where no image analysis can be used, a specific apparatus has been built: a plume of rising bubbles is generated and filmed in water or in organic solvent (cyclohexane in this work) in very different conditions depending on gas flow rate. Bubbles may be distorted and deviated under the action of the neighbouring wakes. Bubble velocities and sizes are separately evaluated by means of optic probe technique and image analysis. The influence of bubble lateral motion and of bubble proximity and distortion is checked. For the optic probe technique, the signal treatment procedure is reconsidered for the determination of bubble velocity and size, and the consistence of the delivered data is discussed.

2. Optic probe signal: principle and classical treatment

Gas-phase characterization by use of optic probes is a well-known technique: an infra-red light is generated from an opto-electronic apparatus and is injected into a glass fibre; this light sweeps along the fibre to the tip. The probe tip is located in the flow at the measuring point. The flux of light is partially refracted into the fluid around the fibre tip. The rest is reflected back to the opto-electronic apparatus. The amount of light that sweeps back to the apparatus depends on the refractive index of the fluid surrounding the fibre tip (Snell law): if the tip lies in gas, a large fraction of the light intensity is returned. If the probe faces rising bubbles, it delivers a square-pulsed signal, whose high parts correspond to gas phase and low parts to liquid phase. Gas and liquid parts of the signal are segregated by use of a threshold on raw data (Fig. 1). Gas hold-up is the cumulative gas part on signal, referred to total signal length.

In order to reach bubble velocities and diameters, two optic fibres can be mounted together into a double probe (Fig. 2). In this case, the tips must be close (distance l_{12}) and
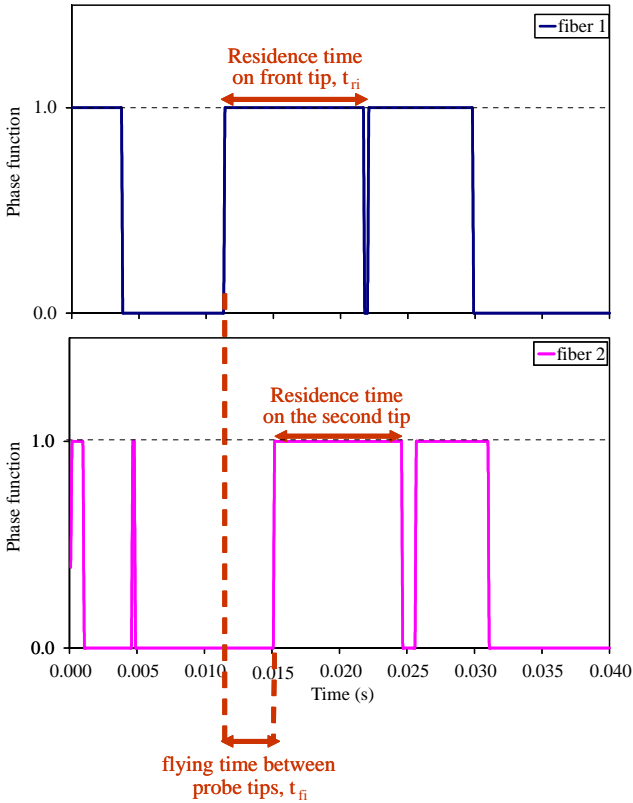
Fig. 2. Double optic probe.

Fig. 3. Binarised signal and crenels association.

aligned with the direction of bubble rise. The two signals are acquired simultaneously. The transit of a bubble on each tip generates a pulse on each signal; pulses of the two raw signals have to be associated in corresponding pairs (see Fig. 3: binarized signals corresponding to Fig. 1), so that bubble flying times between probe tips, t_{fi}, can be determined, leading to individual bubble velocities, v_{bi}:

$$v_{bi} = \frac{l_{12}}{t_{fi}}. \tag{1}$$

Note that v_{bi} can be considered as the axial velocity of bubble centre of mass if rise velocity is parallel to l_{12} and if bubbles suffer no deformation, deviation or rotation during their flight from tip to tip.

Once bubble velocities are known, bubble residence times on front fibre tip, t_{ri}, can be converted into bubble chords:

$$c_{bi} = v_{bi}.t_{ri}. \tag{2}$$

The chord distribution may be statistically transformed into a diameter distribution assuming spherical or ellipsoidal shape for bubbles (Werther, 1974; Turton and Clark, 1989; Clark et al., 1996); this assumption corresponds to small bubbles (1–3 mm).

Association of pulses is a crucial and difficult stage of signal treatment. The usual procedure is the following:

- Let τ_{max} be the most probable flying time for bubbles to go to front tip to rear tip. τ_{max} is the maximum of the raw signals inter-correlation function. In this work, the inter-correlation coefficient is found significantly high (between 0.79 and 0.84).
- For each crenel observed on front tip signal at time t, a crenel is searched on rear tip signal within a time interval $[t + a\tau_{max}; t + b\tau_{max}]$, where coefficients a and b are usually chosen equal to 0.5 and 1.5, respectively (Kamp, 1996).

The treatment of optic probe signals leads then to two distinct average values for bubble axial velocity: the arithmetical mean of v_{bi} values, $\overline{v}_{ax,probe}$, and the most probable velocity of bubbles between probe tips, $\tilde{v}_{ax,probe}$, are defined as:

$$\tilde{v}_{ax,probe} = \frac{l_{12}}{\tau_{max}}. \tag{3}$$

3. Experimental set-up and procedure

3.1. Set-up

A specific glass tank, called 'aquarium', was built (Fig. 4). This tank is square (section: $0.25\,m \times 0.25\,m$, height: $0.50\,m$); it is filled with liquid (water or cyclohexane). The aquarium can be fed with air or nitrogen through two single-hole distributors (hole dimension: $0.001\,m$, inter-hole distance: $0.04\,m$). The optic probe is settled through the aquarium wall so that the front tip is situated in the plume of bubbles at $0.2\,m$ above the distributors. Gas flow rate is varied between 8×10^{-4} and $4 \times 10^{-3}\,L/s$ to get different bubbling conditions. Bubble size and bubbling frequency may be varied in large ranges leading to very different interactions and resulting in various bubble shapes and paths.

3.2. Techniques

The probe used for this study is a commercial double optic sensor (RBI, Fig. 2). The tip diameter is around $40\,\mu m$ and the inter-tip distance l_{12} is $0.0020\,m$. Front tip and rear tip signals are acquired under a sampling frequency of $10\,kHz$ and a recording time of $200\,s$. In these conditions a record leads to more than 1000 bubbles detected by the probe front

Fig. 4. Experimental set-up.

tip, whatever the gas flow rate. At this sampling frequency the intrinsic precision of the method is good: the maximum signal method error is less than 10% on t_{ri} for $t_{ri} > 1 \times 10^{-3}$ s, and less than 5% on v_{bi} for $v_{bi} < 1$ m/s. But note that this precision decreases at short bubble residence time (or flying time). The lower detection limit of chord length depends on bubble velocity: $c_{b \min,i} = v_{bi}/f_{\text{sampling}} = 10^{-4} v_{bi}$, that is to say 0.1 mm for $v_{bi} = 1$ m/s. It has to be noted that, in this section, classical problems like partial wetting of the probes or liquid films hanging on to the probes (Cartellier and Barrau, 1998) are neglected: those effects are insignificant with regard to the following ones.

A high-speed camera (CMOS monochrom, New Vision Technologies NV1000 system), placed in front of the glass column, registers bubble rise (Fig. 4). Pictures are numerically analyzed with the Visilog 5.2 software on the basis of bubble projected area.

For velocity measurements, a large visualisation window is used (dimension: 0.07 m × 0.07 m centred on the bubble train path), that shows the tips of the optic probe (Fig. 5, a–d). The sampling frequency is 51.44 pictures/s. In these conditions, each bubble appears on four consecutive pictures at least. The axial and radial components of bubble velocity, $v_{ax,\text{photo}}$ and $v_{\text{rad,photo}}$, are determined through the position of bubble centre of mass (based on projected area). To derive the mean values of these components ($\overline{v}_{ax,\text{photo}}$ and $\overline{v}_{\text{lat,photo}}$), 150 values of velocity at least are used. Based on the resolution of the technique (54 pixels for 0.0040 m), the minimum intrinsic precision of image analysis for velocity measurement is 0.8%.

For accurate bubble size measurements, the visualisation window is smaller (0.02 m × 0.03 m). A sampling frequency of 30 pictures/s is used. For each bubble, the equivalent diameter is determined (diameter of the sphere of equivalent projected area). The mean equivalent diameter is derived on the basis of 150 different bubbles at least. In this case the resolution of the technique (250 pixels for 0.0119 m) implies that the minimum intrinsic precision for the measurement of equivalent diameter is 0.2%. Note that, when bubble concentration is high, bubble projections over-lapping occurs on pictures. Bubbles contours are therefore difficult to determine automatically and bubbles have to be checked one by one by the human eye. This explains the moderate numbers of analyzed bubbles.

3.3. Description of the bubble flows tested

The aquarium is first filled with water; the four conditions of operation (referred to as cases 1, 2, 3 and 4 in the following) are presented (Fig. 5). The corresponding mean bubbling frequencies f_B (registered at probe location) stand between 3 and 10 bubbles/s.

In case 1 (Fig. 5a) a regular train of bubbles is obtained; bubble sizes and shapes are quite uniform and bubble rise is almost vertical. In cases 2 and 3 (Figs. 5b and c), the plume is larger: bubbles motion shows a lateral velocity component; some bubbles cluster, and various sizes can be observed. In case 3 very small bubbles as well as large and distorted bubbles rise together. In case 4 (Fig. 5d), groups of bubbles still exist (bubble concentration may be very high), and very large bubbles (more than 1 cm in characteristic size) are observed.

Due to increasing plume oscillations and radial dispersion of bubbles (from case 1 to 4), mean bubbling frequency gets underestimated by the probe and is less related to bubble formation frequency (at the orifice).
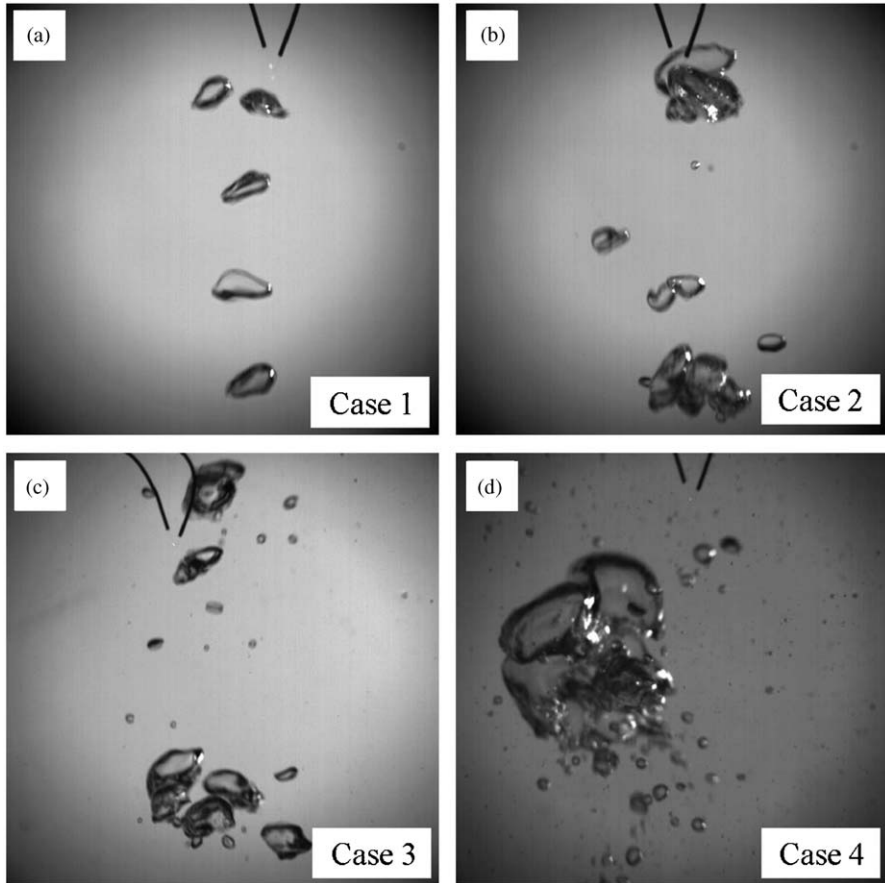
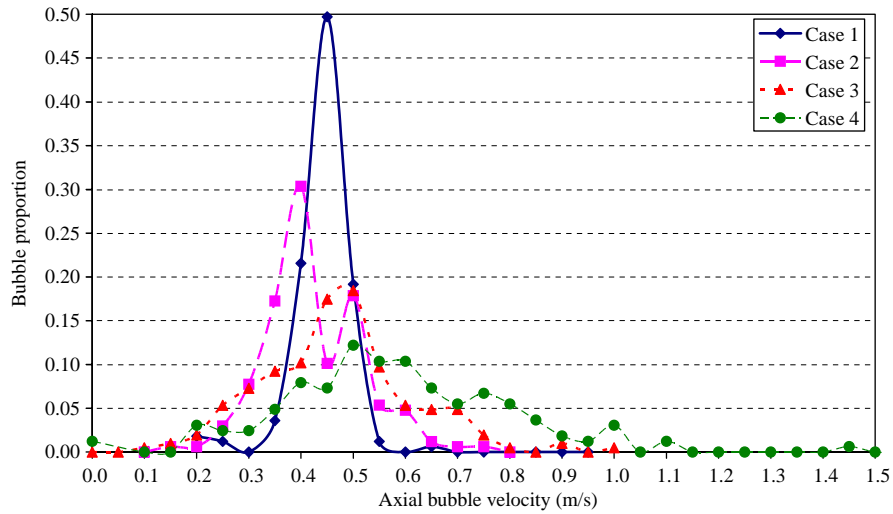Fig. 5. Photos obtained for the 4 cases studied for velocity measurement (water).

Fig. 6. Axial velocities PDF of bubble velocities (derived from photos).

To confirm visual observations, the Probability Density Functions in axial and radial components of bubble velocity are presented in Figs. 6 and 7, respectively. These data are obtained by image analysis. The shown PDFs are large and their widths increase with gas flow rate; in case 4, some

values of radial velocity reach the magnitude of mean axial velocity.

These four bubble flows are used for the study of bubble velocities; for size analysis, three similar bubble flows are generated in water (measured values of f_B between 1.8 and
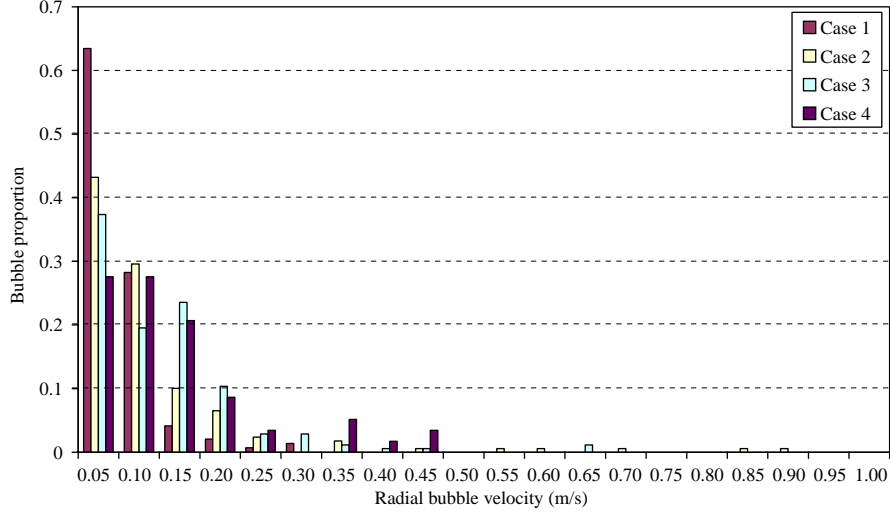
Fig. 7. Radial velocities PDF of bubble velocities (derived from photos).

5.4 bubbles/s) and in cyclohexane (measured values of f_B between 1.6 and 5.1 bubbles/s).

The investigation of these bubble flows is then expected to quantify the error made on bubble velocity and bubble size evaluation by the probe technique.

4. Results and discussion

Note that only statistical data obtained with the two techniques may be compared, as filmed bubbles cannot be individually recognized on probe signals: it is impossible on 2D films to establish if a bubble has touched the optic fibre or not.

4.1. Bubble velocity

Table 1 compares the mean value of axial velocity, $\overline{v}_{ax,\text{photo}}$, measured by image analysis, and the most probable axial velocity, $\tilde{v}_{ax,\text{probe}}$, evaluated by the probe technique. The agreement is rather good, nevertheless probe velocity estimations are higher and discrepancies increase with gas flow rate: in case 4 the deviation between the two techniques reaches 31.7%.

Distributions of axial velocity are compared in Fig. 8. For the probe technique, signal treatment is performed with $a = 0.5$ and $b = 1.5$ (cf. §2). Note that for the extreme cases 1 and 4, distributions corresponding to several distinct optic probe records show good repeatability of the technique, for these types of bubble flow.

For cases 1 and 2, the two PDF curves are sharp and centred on 0.48 m/s. The agreement between the two methods (camera and optic probe) is satisfying, even if the probe technique systematically leads to higher values of velocities (between 0.6 and 1 m/s). This observation can be partially attributed to the relatively high lateral component of bub-

Table 1
Comparison of bubble axial velocities derived by both techniques (probe technique: $a = 0.5$, $b = 1.5$)

	Case 1	Case 2	Case 3	Case 4
Bubble frequency (bubbles/s) (optic probe)	4.6	2.9	5.3	9.9
Bubble number treated by photo analysis	167	169	206	164
Associated bubble number (optic probe)	807	575	576	1041
$\overline{v}_{ax,\text{photo}}$ (m/s)	0.415	0.396	0.455	0.562
$\overline{v}_{ax,\text{probe}}$ (m/s)	0.474	0.478	0.556	0.795
$\tilde{v}_{ax,\text{probe}}$ (m/s)	0.460	0.480	0.560	0.740
$\tilde{v}_{ax,\text{probe}}/\ \overline{v}_{ax,\text{photo}}$ deviation	10.8%	21.21%	23.1%	31.7%
$\overline{v}_{ax,\text{probe}}/\ \overline{v}_{ax,\text{photo}}$ deviation	14.2%	20.7%	22.2%	41.5%
$\tilde{v}_{ax,\text{probe}}/\ \overline{v}_{ax,\text{probe}}$ deviation	3.0%	0.4%	0.7%	7.1%

ble motion, leading to short flying times of bubbles between probe tips: as bubble movement is not parallel to l_{12}, bubble curvature leads to a weak flying time (Fig. 9). To take this effect into account, residence times on the two fibres should be compared: a priori, the more different the two values are, the greater the lateral motion is (Fig. 9). Fig. 10 presents the pdf curves of this difference for cases 1 and 2: most bubbles have a little residence time difference between the two probes (probably because of the low value of l_{12}). Moreover, if only the bubbles having low difference values are considered, some bubbles are rejected, but high velocity values remain. This criterion helps to characterize the flow, but it is not sufficient to improve the treatment.
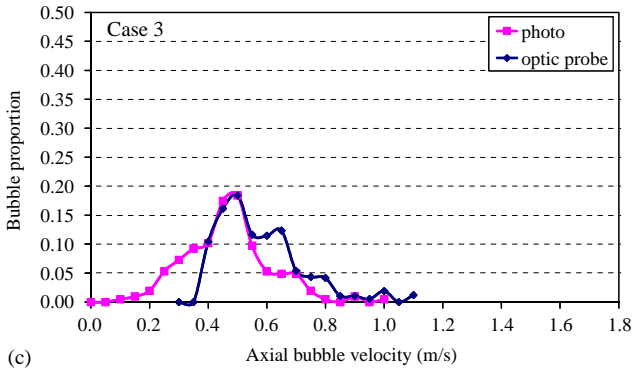
As gas flow rate increases, PDF curves in axial velocity get larger and flatter (Fig. 8). This is consistent with the observed distorted bubble shapes and paths. The
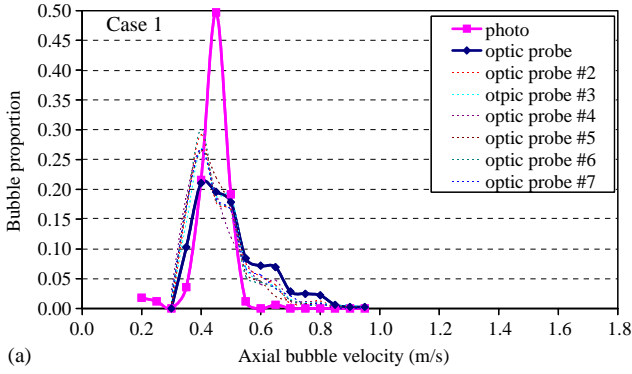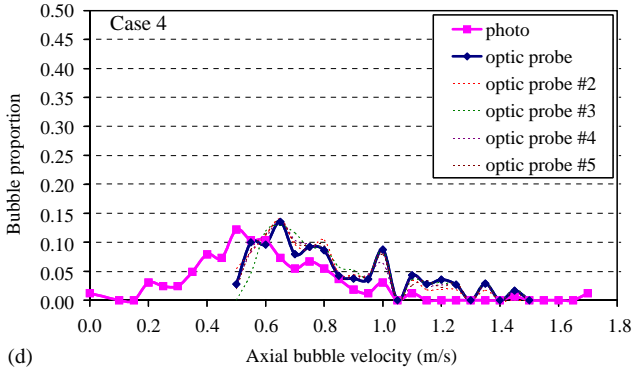
(a)
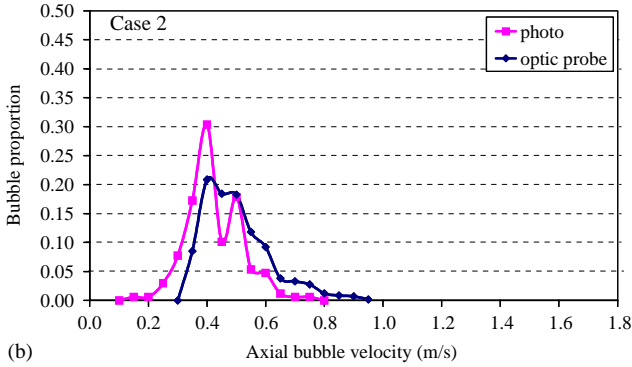
(b)

(c)

(d)

Fig. 8. Comparison of velocities PDF derived by both metrologies (photo and optic probe).

distributions provided by the probe technique appear to be cut at low values: coefficient $b=1.5$, used in signal treatment to restrict the search interval for bubble association, is too small, prohibiting low velocities measurement.
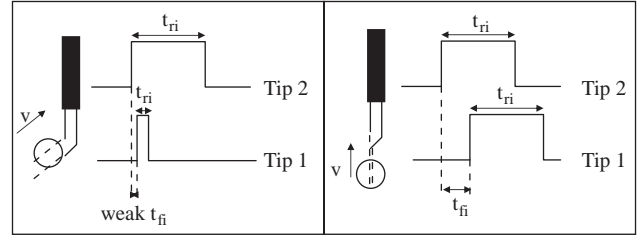

Fig. 9. Problem for radial velocity derivation.

As a consequence, the arithmetic average of bubble axial velocities, $\overline{v}_{ax,\mathrm{probe}}$, is higher than the mean axial velocity of reference, $\overline{v}_{ax,\mathrm{photo}}$; the deviation reaches 41.5% in case 4. The two velocity evaluations provided by the probe technique, arithmetic average $\overline{v}_{ax,\mathrm{probe}}$ and most probable velocity $\tilde{v}_{ax,\mathrm{probe}}$ are not equivalent; $\tilde{v}_{ax,\mathrm{probe}}$, which is not affected by association problems, seems to be more reliable.

In order to improve $\overline{v}_{ax,\mathrm{probe}}$ values, signal association should be revised. As fitting a and b is equivalent to set the extreme velocities, a and b coefficients are adjusted to obtain the same velocity interval with the optic probe and with the camera. Case 4 is presented in Fig. 11: for $a=0.4$ and $b=3.7$ the agreement between the two methods becomes excellent. For the other cases, values of adjusted coefficients a and b and corresponding $\overline{v}_{ax,\mathrm{probe}}$ data are reported in Table 2. Whatever the case, the arithmetic average value $\overline{v}_{ax,\mathrm{probe}}$ is now closer to the reference velocity $\overline{v}_{ax,\mathrm{photo}}$.

Coefficients a and b cannot be optimized a priori for measurements in opaque reactors. Table 2 shows, however, that $a=0.5$ is satisfying for the 4 cases considered (the maximum velocity does not exceed $2\tilde{v}_{ax,\mathrm{photo}}$), and that high values of b have to be checked. However, if high values of b admit low velocity values, it might also lead to wrong pulse association at higher bubble frequency: the pulses associated could be induced by two different bubbles.

The test of several values of a and b (Fig. 12) proves that a change in a and b modifies the width of velocity PDF but not its shape. Bubble association is conveniently performed whatever the selected screening time.

As a conclusion, the optimal coefficients a and b to be used by probe signal treatment are specific to the bubble flow studied; it seems reasonable to keep the classical value of $a = 0.5$ and to let b exceed 1.5 (for weak bubble frequency). In opaque reactors, the optimum value of b cannot be determined: the arithmetic average of individual bubble velocities cannot be fully trusted and the most probable velocity, deduced from signals inter-correlation, is a priori a correct estimation for bubble axial velocity.

4.2. Bubble size

4.2.1. Reliability of bubble chords distribution

To estimate bubble chords with probe technique, it is usually needed to know the bubble residence time and
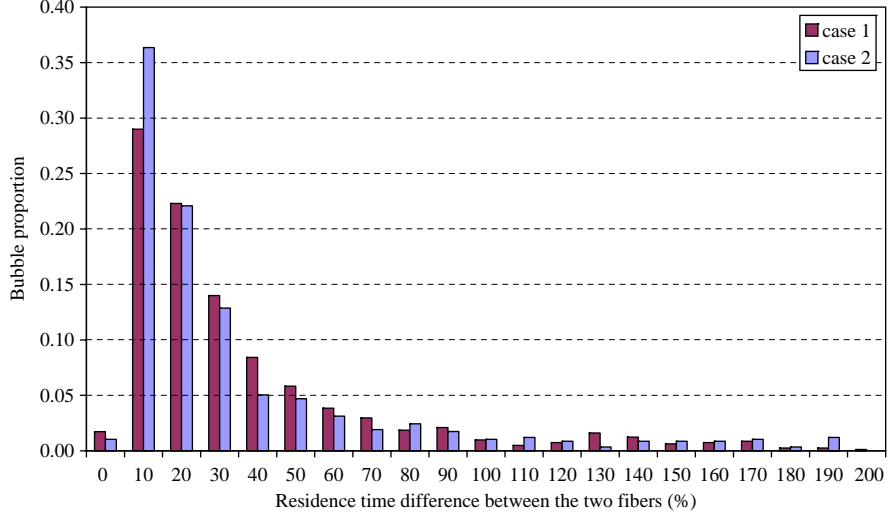
Fig. 10. PDF of differences between residence time on the two tips (cases 1 and 2).
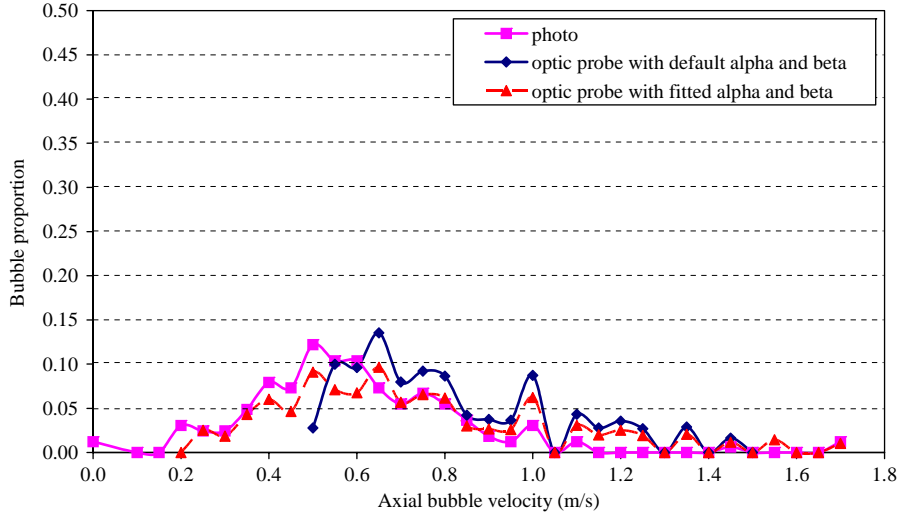

Fig. 11. Effect of adjustment of *a* and *b* on velocity PDF issued from photo (case 4).

Table 2
Comparison of bubble axial velocities derived by both techniques (probe technique: adjusted coefficients *a* and *b*)

	Case 1	Case 2	Case 3	Case 4
$\tilde{v}_{ax,\mathrm{probe}}$ (m/s)	0.46	0.48	0.56	0.74
$\overline{v_{ax,\mathrm{photo}}}$ (m/s)	0.415	0.396	0.455	0.562
α	0.75	0.6	0.5	0.4
β	2.5	2.4	278	3.7
$\overline{v_{ax,\mathrm{probe}}}$ (m/s)	0.427	0.447	0.477	0.706
$\tilde{v}_{ax,\mathrm{probe}}/\overline{v_{ax,\mathrm{probe}}}$ deviation	7.1%	7.1%	16.0%	4.7%
$\overline{v_{ax,\mathrm{probe}}}/\overline{v_{ax,\mathrm{photo}}}$ deviation	2.79%	12.8%	4.8%	25.6%

the individual bubble axial velocity for each treated bubble (Revankar and Isshii, 1992; Kalkach-Navarro et al., 1993).

The measurement of bubble residence times on a tip is direct (Fig. 3; see Fig. 13 as example of bubble residence time PDF for tip 1), but it was shown in Section 4.1. that the distribution of individual axial velocities derived by the probe technique depends on coefficients *a* and *b*. So we may wonder if it is possible to calculate a significant chord distribution with partial PDF in velocities.

For the bubbles flows tested in this work, no correlation can be found between velocity module and bubble equivalent diameter (Fig. 14), nor between axial velocity and equivalent diameter (Fig. 15) (data issued from photos). Therefore, a fraction of axial velocity PDF should a priori lead to all values of chords for this bubble population: whatever the *a* and *b* values, the chord PDF is not affected. This trend is verified on chord PDF curves (established with tip 1) derived for case 4 presented in Fig. 16 for three sets of values of *a*
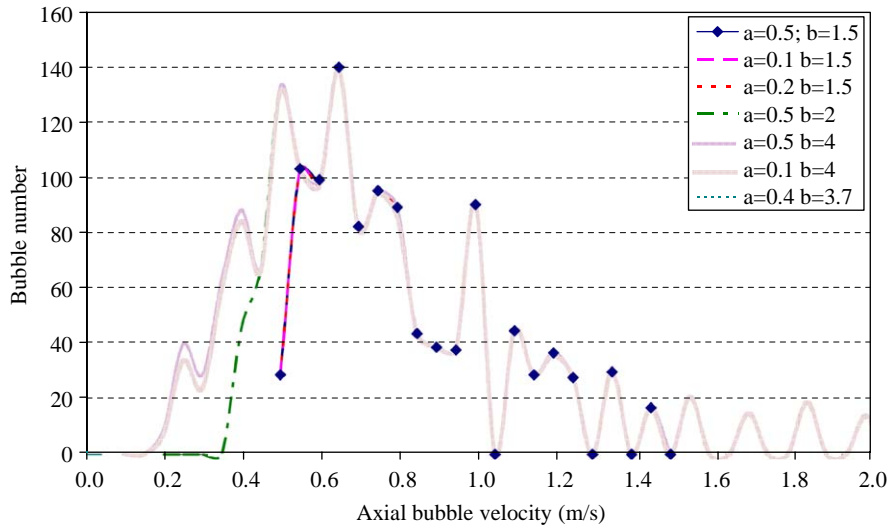
Fig. 12. Number distributions of axial velocity derived from different values of *a* and *b* (case 4).
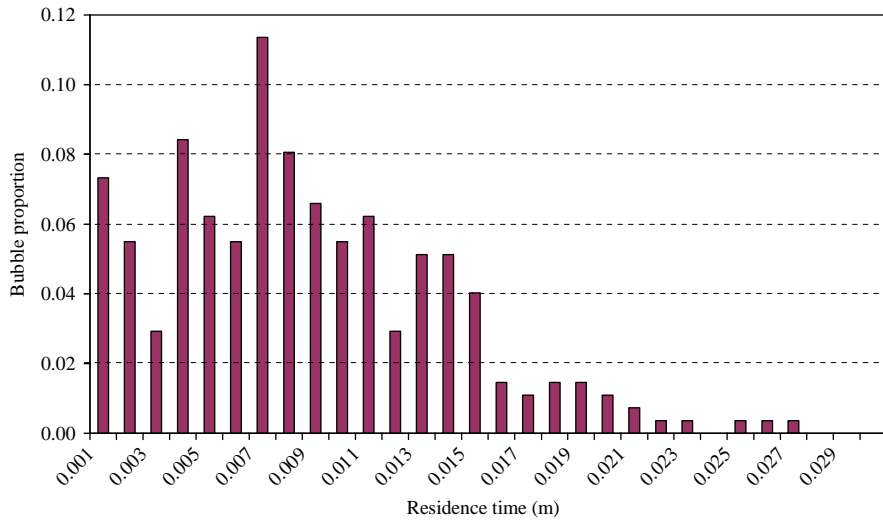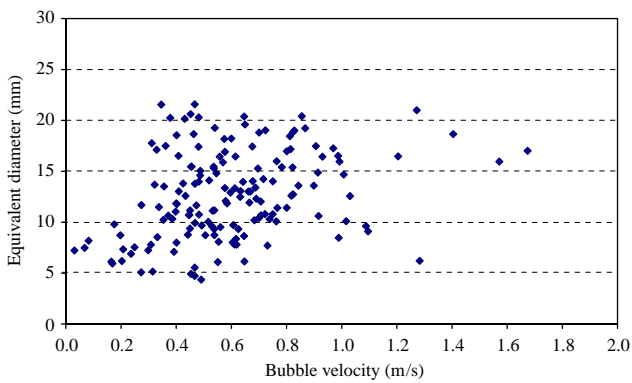

Fig. 13. Example of residence time PDF.

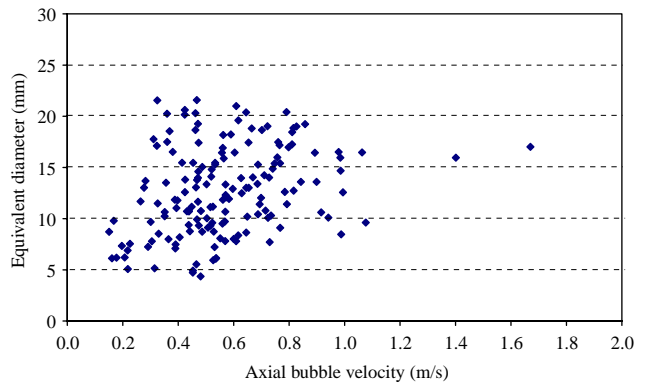Fig. 14. Evolution of equivalent diameter with bubble velocity module (case 4).

Fig. 15. Evolution of equivalent diameter with bubble axial velocity (case 4).
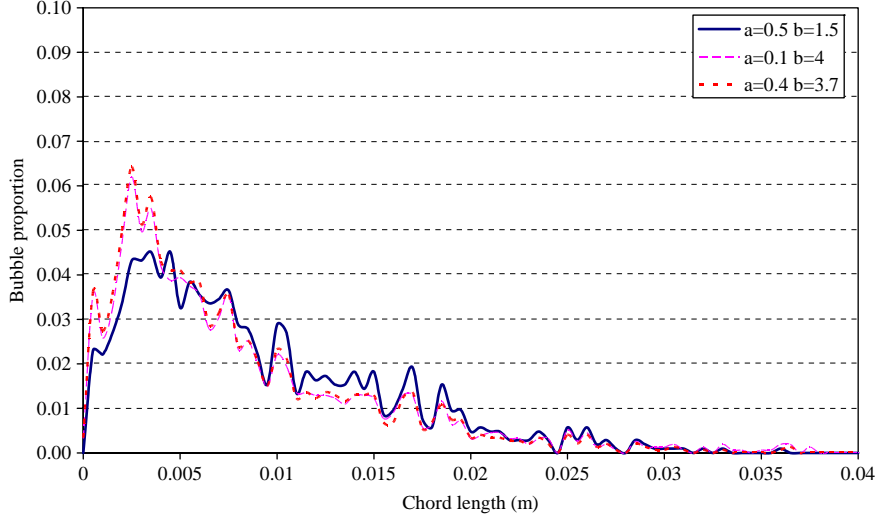
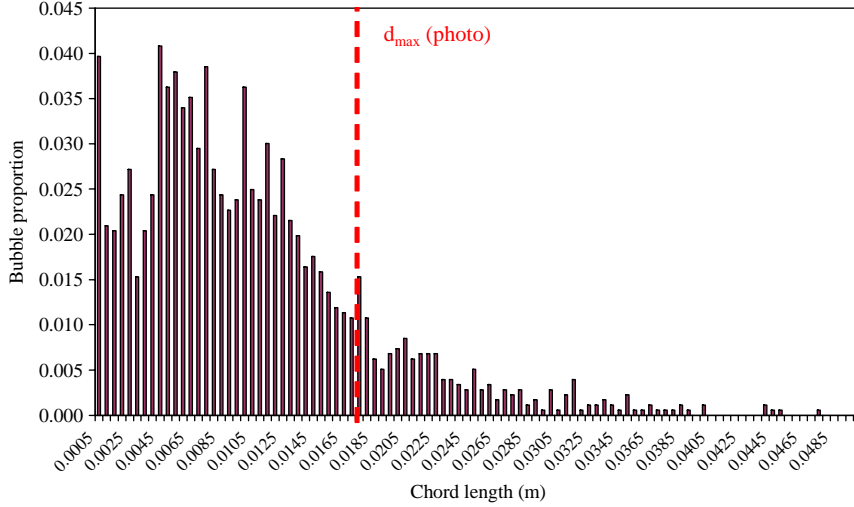Fig. 16. Chord PDF derived from different values of *a* and *b*.

Fig. 17. Chord PDF (cyclohexane, case 3).

and *b*: the shapes of PDF curves are similar; *a* and *b* have only a little influence on chord distributions.

4.2.2. Bubble size estimation

For this part of the work, specific tests are performed in water and in cyclohexane. For each liquid medium three bubble flows are analysed. For probe treatment, *a* and *b* values are equal to 0.5 and 1.5, respectively.

To convert bubble chord distribution into diameter distribution, the maximum value of chord PDF is commonly considered as the maximum value of diameter PDF (Kamp, 1996).

Compared to the maximum equivalent diameter issued from the photo (Fig. 17, cyclohexane, case 3), the chord distribution shows too many high values: more than 15% of chord values are greater than d_{max}. The distorted shapes and

the chaotic motion of bubbles are probably responsible for these non-consistent chord measurements: the bubble may slow down, change its path and/or shape when crossing the probe tip. Then it is not realistic to derive chord distribution with probe technique, for tumbling or deformed bubbles.

When significant distributions are not available, some authors (Kalkach-Navarro et al., 1993) use an empirical relation between the mean chord length and the mean equivalent diameter:

$$d_{10} = \lambda c_{10}, \qquad (4)$$

where c_{10} is the mean chord (first moment of chord PDF), and where λ is a parameter that depends on local flow characteristics. Experimental values of λ stand around 1.5 for nearly spherical bubbles. In the present study λ decreases at increasing flow rate and ranges between 0.3 and 1.4. As

Table 3
Comparison of estimated bubble size derived by both techniques

	Case	$\tilde{v}_{ax,\text{probe}}$ (m/s)	$d_{SM,\text{photo}}$ (m)	$d_{SM,\text{ Eq. (5)}}$ (m)	Deviation
Cyclohexane	1	0.57	0.0036	0.0034	5.5%
	2	0.80	0.0058	0.0053	9.3%
	3	1.17	0.0066	0.0101	42.6%
Water	1	0.73	0.0069	0.0056	20.2%
	2	0.88	0.0062	0.0070	11.6%
	3	1.20	0.0094	0.0123	27.1%

a consequence, chord distributions cannot be used even for average diameter estimation.

To avoid the use of chord distributions, another approach, using only mean values, is expected. A simplified relation is derived to estimate the bubble Sauter diameter on the basis of the work of Ishii and colleagues (Kataoka et al., 1986), dedicated to the determination of the local average interfacial area by probe technique:

$$d_{SM} = \frac{3\tilde{v}_{ax,\text{probe}}\varepsilon_G}{2f_B}, \tag{5}$$

where d_{SM} is the mean Sauter diameter of the bubble population.

This relation uses the most reliable measured parameters only: gas hold-up ε_G, bubble frequency f_B and most probable axial velocity $\tilde{v}_{ax,\text{probe}}$. For this method, problematic pulse association is not necessary.

Table 3 compares the mean Sauter diameters estimated by image analysis or probe technique (relation (5)) for bubble flows in water and cyclohexane. The agreement is satisfying for cases 1 and 2. When bubbling frequency (or bubble concentration) increases (cases 3), relation (5) seems to overestimate d_{SM} by more than 20%.

5. Conclusion

In this work, the reliability of the optic probe technique is investigated in a specific set-up where trains of distorted and tumbling bubbles are generated.

It is shown that the most probable velocity, deduced from raw signals inter-correlation, is a convenient estimation for axial component of bubble barycenter velocity. Whatever the coefficients used for crenels association, the central part of velocity distribution is representative, but the low and high parts of velocity PDF are not reliable, due to the lateral motion of bubbles or due to their distorted shapes.

The chord PDF deduced from velocity PDF, cannot be trusted. However, a correct estimation of the mean bubble Sauter diameter can be obtained through relation (5), using the most reliable estimated parameters and avoiding hazardous pulse association. This estimation has been validated

with two liquid media, water and cyclohexane, even with highly distorted and tumbling bubbles.

Nevertheless, in industrial reactors, bubbles experience large liquid loops and intense shear stress. The signal treatment associated with the probe technique is still more critical and has to be specifically investigated. This work is under progress in a large bubble column.

Notations

Abbreviations

PDF — probability density function

Symbols

a	coefficient leading to the low screening limit for crenels associations, dimensionless
a_i	coefficient leading to the high screening limit for crenels associations, dimensionless
b	interfacial area, m^2/m^3
c_{bi}	chord length of bubble i, m
$c_{b\,\text{min},i}$	minimum chord length of bubble i, m
c_{10}	mean chord length, m
d_{10}	bubble mean diameter, m
d_{SM}	mean Sauter diameter, m
f_B	bubble frequency, s^{-1}
f_{sampling}	signal acquisition frequency, s^{-1}
l_{12}	inter-tip distance, m
t	time, s
t_{fi}	flying time of bubble i, s
t_{ri}	residence time of bubble i, s
v_{bi}	axial velocity of bubble i, m/s
$\overline{v}_{ax,\text{photo}}$	mean axial bubble velocity measured by photo, m/s
$\overline{v}_{ax,\text{probe}}$	mean axial bubble velocity measured by optic probe, m/s
$\tilde{v}_{ax,\text{probe}}$	most probable bubble velocity measured by probe, m/s
$v_{\text{rad,photo}}$	lateral bubble velocity measured by photo, m/s

Greek letters

ε_G	gas hold-up, dimensionless
λ	proportionality coefficient between c_{10} and d_{10}, dimensionless
τ_{max}	most probable flying time, dimensionless

References

Boyer, C., Cartellier, A., 1999. Bubble velocity and size estimation using a single optical probe in a gas/liquid flow across a fixed bed reactor. Récents Progrès en Génie des Procédés 13, 379–386.

Boyer, C., Duquenne, A.M., Wild, G., 2002. Measuring techniques in gas–liquid and gas–liquid-solid reactors. Chemical Engineering Science 57, 3185–3215.

Cartellier, A., Barrau, E., 1998. Monofiber optical probes for gas detection and gas velocity measurements: conical probes. International Journal of Multiphase Flow 24, 1265–1294.

Clark, N.N., Liu, W., Turton, R., 1996. Data interpretation techniques for inferring bubble size distribution from probe signals in fluidized systems. Powder Technology 88, 179–188.

Ellingsen, K., Risso, F., 2001. On the rise of an ellipsoidal bubble in water: oscillatory paths and liquid-induced fluctuations. Journal of Fluid Mechanics 440, 235–268.

Kalkach-Navarro, S., Lahey, R.T., Drew Jr., D.A., Meyder, R., 1993. Interfacial area density, mean radius and number density measurements in bubbly two-phase flow. Nuclear Engineering and Design 142, 341–351.

Kamp, A., 1996. Ecoulements turbulents á bulles dans une conduite en micropesanteur. Ph.D. Thesis, INPT, France.

Kamp, A., Colin, C., Fabre, J., 1995. Techniques de mesure par sonde optique double en écoulement diphasique à bulles. Colloque de Mécanique des Fluides Expérimentale, Cert Onera, Toulouse, France.

Kataoka, I., Ishii, M., Serizawa, A., 1986. Local formulation and measurements of interfacial area concentration in two-phase flow. International Journal of Multiphase Flow 12, 505–529.

Kiambi, S.L., Duquenne, A.M., Dupont, J.B., Colin, C., Risso, F., Delmas, H., 2003. Analysis of bubble-probe interactions by imaging: application to local interfacial measurements. Canadian Journal of Chemical Engineering 81, 764–770.

Revankar, S.T., Ishii, M., 1992. Local interfacial measurement in bubbly flow. Internatinal Journal of Heat and Mass Transfer 35, 913–925.

Turton, R., Clark, N.N., 1989. Interpreting probe signals from fluidized beds. Powder Technology 59, 117–123.

Werther, J., 1974. Bubbles in gas fluidized beds. Part I. Transactions of the Institute of Chemical Engineering 52, 149–159.